Journal of Solid State Chemistry 184 (2011) 1036–1042

Contents lists available at ScienceDirect

Journal of Solid State Chemistry

journal homepage: www.elsevier.com/locate/jssc

Optical properties of green-blue-emitting Ca-α-Sialon:Ce^{3+},Li^{+} phosphors for white light-emitting diodes (LEDs)

Hui-Li Li [a,*], Guo-Hong Zhou [b], Rong-Jun Xie [c], Naoto Hirosaki [c], Xiao-Jun Wang [a], Zhuo Sun [a]

[a] Engineering Research Center for Nanophotonics and Advanced Instrument, Ministry of Education, Department of Physics, East China Normal University, Shanghai 200062, China
[b] Structural Ceramics Center, Shanghai Institute of Ceramics, Chinese Academy of Sciences, Shanghai 200050, China
[c] Nano Ceramics Center, National Institute for Materials Science, Namiki 1-1, Tsukuba, Ibaraki 305-0044, Japan

ARTICLE INFO

Article history:
Received 18 January 2011
Received in revised form
25 February 2011
Accepted 5 March 2011
Available online 15 March 2011

Keywords:
Ca-α-Sialon
Phosphor
Cerium
Photoluminescence
White LED

ABSTRACT

Ce^{3+},Li^{+}-codoped Ca-α-Sialon phosphors with the formula $[Ca_{(1-2x)}Ce_xLi_x]_{m/2}Si_{12-(m+n)}Al_{m+n}O_nN_{16-n}$ ($0 \le x \le 0.25$, $0.5 \le m \le 3.5$, and $0.16 \le n \le 2.0$) have been synthesized by gas pressure sintering (GPS). The effects of the activator concentration and the overall composition of host lattice on the phase evolution, morphology, and optical properties were investigated. The single-phase Ca-α-Sialon: Ce^{3+},Li^{+} can be synthesized at $x < 0.1$, $1.0 \le m \le 2.5$, and $n \le 1.2$. The synthesized powders exhibit a relatively dispersive and uniform morphology. Under the near UV excitation, the bright green-blue emission centered at 500–518 nm is observed. The photoluminescence can be tailored by controlling Ce^{3+} concentration and the overall composition of the α-Sialon host lattice. With increasing the Ce concentration and m value both excitation and emission bands show a red shift, which perfectly matches with the near-UV LEDs in the range of 360–410 nm. The strongest luminescence is achieved at $x=0.08$–0.1, $m=2.0$–2.5, and $n=1.0$. Simultaneously, the highest quantum efficiency and better thermal stability are also present.

1. Introduction

In recent years, divalent europium activated M-α-Sialon ($M^{val+}_{m/val+}Si_{12-(m+n)}Al_{(m+n)}O_nN_{(16-n)}$, where "val" is the valence of the metal ion, M=Ca, Li, or Y) have attracted much attention due to their nontoxicity, high thermal stability, and excellent luminescence properties as conversion phosphors for white light-emitting diodes (LEDs) [1–12]. Specifically for M=Ca, Ca-α-Sialon: Eu^{2+} shows a superior absorption in the spectral region between 280 and 470 nm and a broad yellowish orange emission from 550 to 600 nm because of the large crystal-field splitting and strong nephelauxitic effect caused by the coordination of europium ions to nitrogen. When it was coupled to a blue LED chip, the warm-white LED lamps with the tailoring of correlated color temperatures (CCTs) from 2640 to 3020 K can be obtained [5,13], which is required for the interior illumination. α-Sialon-based oxynitride phosphors offer the following features and therefore are of technological and scientific importance: ① strong absorption in the visible light spectral region and long wavelength emission; ② flexibility in material design since their composition varies over a broad range without changing the crystal structure; and ③ chemical and thermal stability as their basic structure is based on tetrahedral, either of the Si–(O, N) or Al–(O, N) type [14].

Similar to Eu^{2+}, Ce^{3+}-activated phosphors commonly exhibit broadband emission in the UV and visible ranges due to the $4f^0 5d^1 \rightarrow 4f^1$ transition of Ce^{3+} and their luminescence decays are fast [15–20]. Usually, the trivalent cerium ion with the electronic configuration $4f^1$ has $^2F_{7/2}$ and $^2F_{5/2}$ manifolds as the ground states are separated by $\sim$2000 cm^{-1} due to spin-orbit coupling. The lower manifold $^2F_{5/2}$ is populated and the manifold $^2F_{7/2}$ is almost empty at room temperature. The excited configuration is 5d which is split by the crystal-field into 2–5 components. As the positions of the energy levels of 5d excited state of Ce^{3+} are not only affected by the symmetry and strength of the crystal-field but also by the degree of covalent bonding, it causes variations in the absorption and emission from UV to long wavelength by varying the host lattice [21–23]. Therefore, the long-wavelength emission is expected when Ce^{3+} is doped into α-Sialon host lattice with high rigidity caused by a highly condensed $(Si, Al)_{12}(O, N)_{16}$ tetrahedral networks. Photoluminescence of Ce-doped Ca-α-Sialon ceramic and phosphor had been briefly reported by Krevel and Xie et al. [1,24,25], respectively. Unusual long-wavelength emission peaking at 515–540 nm with an intense broad excitation band extending from ultraviolet part to 450 nm was found. This long-wavelength emission is ascribed to the large crystal-field and high covalency of the lattice site due to nitrogen incorporation. The results, simultaneously, indicate

* Corresponding author. Fax: +86 21 622 343 21.
E-mail address: hlli@phy.ecnu.edu.cn (H.-L. Li).

0022-4596/$ - see front matter © 2011 Elsevier Inc. All rights reserved.
doi:10.1016/j.jssc.2011.03.012

that this material is a promising conversion phosphor for white LEDs based on near-UV or blue-emitting LED chips. However, as far as we know, the effects of host lattice composition (i.e., m and n values) and Ce^{3+} concentrations in Ca-α-Sialon on the structural evolution and optical properties have not been carefully investigated.

In this paper, we focus on the influences of Ce^{3+} contents, m and n values variation in Ca-α-Sialon on the structure and luminescence properties of Ca-α-Sialon:Ce^{3+} at room temperature. Quantum efficiency and temperature-dependent luminescence from room temperature to 300 °C were also measured and discussed in detail.

2. Experimental

2.1. Syntheses of undoped and Ce^{3+},Li^{+}-codoped Ca-α-Sialon phosphors

Undoped and Ce^{3+},Li^{+}-codoped Ca-α-Sialon phosphors with compositions of $[Ca_{(1-2x)}Ce_xLi_x]_{m/2}Si_{12-(m+n)}Al_{m+n}O_nN_{16-n}$ ($0 \le x \le 0.25$, $0.5 \le m \le 3.5$, and $0.16 \le n \le 2.0$) were prepared from the mixture of α-Si_3N_4 (SN-E10, Ube Industries, Tokyo, Japan), AlN (Tokuyama Corp., type F, Tokyo, Japan), Al_2O_3 (Taimicron, Daimei Chemicals Co. Ltd., Tokyo, Japan), CeO_2 (Shin-Etsu Chemical Co. Ltd., Tokyo, Japan), $CaSi_2$ (High Purity Chemicals, Japan), $CaCO_3$, and Li_2CO_3 (Kojundo Chemical Laboratory Co. Ltd., Japan) as the starting materials. The Ce^{4+} ions in the starting powder CeO_2 is reduced to Ce^{3+} during sintering [24]. Li^{+} compensates the charge discrepancy caused by the substitution of Ce^{3+} for Ca^{2+}. For each composition, appropriate amounts of the starting powders were weighed out, well mixed and ground in a mortar by hand. Subsequently, they were fired in boron nitride crucible at 1700 °C for 2 h in gas-pressure sintering furnace (FVPHR-R-10, FRET-40, Fujidempa Kogyo Co. Ltd., Osaka, Japan) with a graphite heater under 0.5 MPa N_2 atmosphere. After firing, samples were cooled to room temperature in the furnace and were ground again with an agate mortar for further measurements.

2.2. Structural and morphological characterization

The crystal phase of the fabricated powder was identified by X-ray powder diffraction (XRD, Rigaku RINT2000) using Cu–$K\alpha$ radiation (λ=1.5406 Å) at 40 kV and 40 mA. The data were collected by a normal scan mode with a step size of 0.02° and a scan speed of 2°/min in the range of 2θ of 10–90°. The morphology was examined by a scanning electron microscope (SEM, S-5000).

2.3. Optical measurements

The diffusive reflection spectra were recorded using a UV–vis spectrophotometer with an integrating sphere (JASCO, Ubest V-560). The reflection spectrum of Spectralon diffusive white standards was used for calibration (the reflectivity is nearly 100% in the range of 200–900 nm). The photoluminescence spectra of phosphors were measured at room temperature using a fluorescent spectrophotometer (Hitachi, F-4500) with a 200 W Xe lamp as an excitation source. The quantum efficiency (QE) and temperature-dependent luminescence (25–300 °C) was conducted by using a Hamamatsu MPCD-7000 multichannel photodetector with a 200 W Xe lamp as an excitation source. When the temperature-dependent photoluminescence properties were measured, the powder sample with the size of 10×1 mm^2 was embedded in a hot plate and was then heated to the desired temperature with a heating rate of 100 °C/min. The sample was kept for 5 min to reach thermal equilibrium, which would guarantee a uniform temperature both on the surface and in the interior of sample.

3. Results and discussion

3.1. Phase identification and morphology observation of undoped and Ce^{3+},Li^{+}-codoped Ca-α-Sialon samples

Fig. 1 shows XRD patterns of samples doped with different cerium and lithium concentrations (m=2.0 and n=1.0). It can be seen that a single α-Sialon phase is formed in compositions with $x < 0.1$. The second phase of AlN is identified in the composition of x=0.1, and its relative content gradually increases with the x increasing from 0.1 to 0.2, which suggests that the solubility limit of Ce^{3+} and Li^{+} in α-Sialon is less than 0.1. The obvious variation in diffraction peak positions compared to that of the undoped Ca-α-Sialon indicates lattice shrinkage and incorporation of a smaller size of Ce^{3+}–Li^{+} ion pairs in the α-Sialon lattice (see the inset in Fig. 1).

Fig. 2 gives the XRD spectra of samples with various m and n values and a fixed x value of 0.08. When n value is fixed at 1.0, a single α-Sialon phase is observed at $1.0 \le m \le 2.5$ (Fig. 2(a)). The forming region of α-Sialon in the present work is somewhat narrower than that reported Eu^{2+} activated α-Sialon in the previous work [3,11], which is attributed to different n value, different activator and concentration, and different substitution mechanism between Ce^{3+} and Eu^{2+}. The β-Sialon phase appears and coexists with α-Sialon when m is below 1.0, whereas the AlN phase tends to form when m is over 2.5. In addition, it is clearly seen that the diffraction peak progressively shifts to low diffraction angle with increasing m value (i.e., Ca^{2+} and Ce^{3+}–Li^{+} concentrations), indicating a continuous expansion of the crystal lattice caused by the substitution of the longer Al–N bonds (1.87 Å) for the shorter Si–N ones (1.74 Å). Varying n value and fixing m at 2.0, a single α-Sialon phase is formed in the compositions with low n value ($n < 1.5$). The impurity phase of $SiAl_8O_2N_8$ is observed when $n \ge 1.5$, and also its content increases with n value increasing. Compare Fig. 2(a) with Fig. 2(b), it can be seen that there is no obvious shift for the diffraction peak with increasing n value because the change of the bond length of (Si, Al)–(N, O) caused by the incorporation of the longer Al–O bonds (1.75 Å) is very limited due to a counteraction between shorter Si–O bonds (1.64 Å) and longer Al–O ones.

Fig. 3 shows SEM morphology of a typical Ca-α-Sialon:Ce,Li phosphor (x=0.08, m=2.0, and n=1.0). The powder exhibits

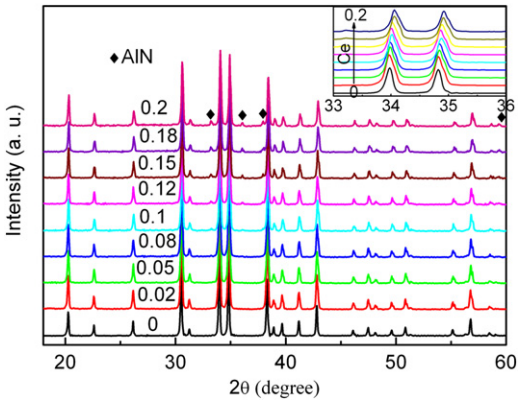

Fig. 1. XRD patterns of samples doped with different amounts of Ce^{3+}, Li^{+} (m=2.0 and n=1.0).

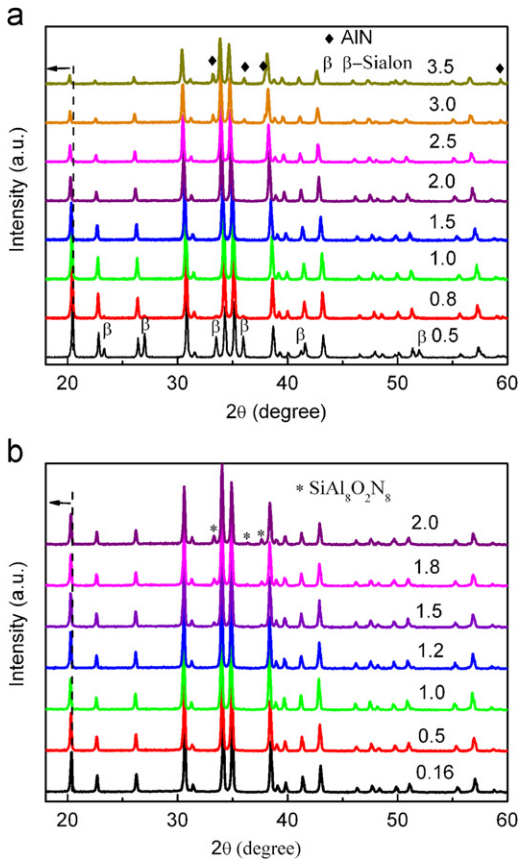

Fig. 2. XRD spectra of samples with $x=0.08$ and various (a) m values ($n=1.0$) and (b) n values ($m=2.0$).

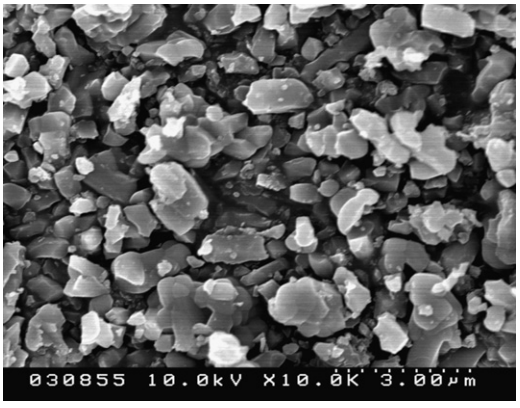

Fig. 3. SEM image of Ca-α-Sialon:Ce,Li phosphor with $x=0.08$, $m=2.0$ and $n=1.0$.

a relatively dispersed and uniform morphology. The particles crystallize well, and the size distributes between 0.3 and 1.5 μm. No obvious and large aggregates are observed. All the characteristics are very required for LED conversion phosphors.

3.2. Diffuse reflection spectra of undoped and Ce^{3+},Li^{+}-codoped Ca-α-Sialon phosphors

UV–visible diffuse reflection spectra of selected samples codoped with different amounts of Ce^{3+} and Li^{+} ions are depicted in Fig. 4. The observed daylight color is white for undoped Ca-α-Sialon. The result is in agreement with the measured diffuse reflection spectrum which shows a high reflection in the visible region and a strong absorption only in the UV part

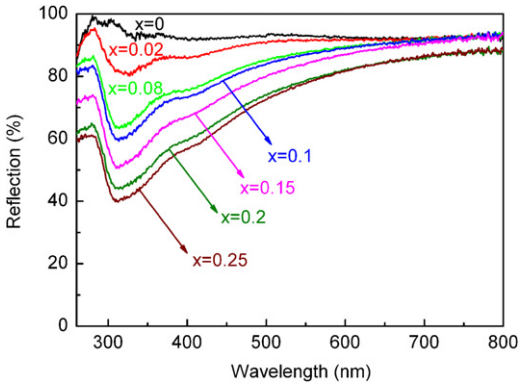

Fig. 4. Diffuse reflection spectra of Ca-α-Sialon:Ce,Li phosphors doped with different cerium concentrations.

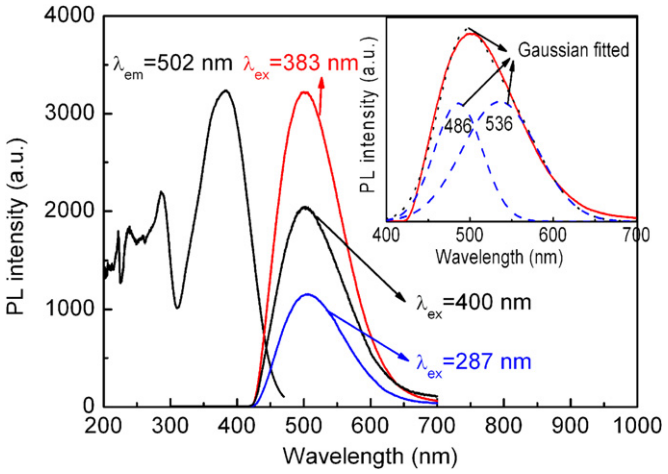

Fig. 5. Excitation and emission spectra of typical Ca-α-Sialon:Ce,Li phosphor with composition of $x=0.08$, $m=2.0$, and $n=1.0$. The inset is the fitted (dot) and decomposed components (dashed) of the emission spectrum ($\lambda_{ex}=383$ nm) by Gaussian deconvolution.

(i.e. <290 nm). The drop in the UV part of reflection curve represents the host lattice absorption from the valence to conduction band. For Ce^{3+},Li^{+}-codoped Ca-α-Sialon, however, a strong absorption band from the UV to the visible region is observed, which can be assigned to the electronic transition from ground state $4f^1$ to excited state of $4f^05d^1$ of Ce^{3+}. Moreover, the absorption becomes stronger with increasing Ce^{3+} concentration. The corresponding color of Ca-α-Sialon:Ce,Li, therefore, varies from white to maize-yellow.

3.3. Photoluminescence properties of Ca-α-Sialon:Ce^{3+},Li^{+} phosphor with $x=0.08$, $m=2.0$, and $n=1.0$

The typical photoluminescent spectra of Ce,Li-codoped α-Sialon phosphor are presented in Fig. 5. The sample shown here has the composition of $x=0.08$, $m=2.0$, and $n=1.0$. The excitation spectrum monitored at 502 nm shows a broadband extending from ultraviolet part to 450 nm. The excitation band at short wavelength in the range of 235–290 nm can be readily assigned to host lattice excitation as indicated by the reflection spectrum (see Fig. 4). The only long wavelength excitation band peaking at 383 nm is caused by $4f\rightarrow5d$ transition of Ce^{3+}. In general, the $5d$ level of Ce^{3+} can be split into at most five different crystal-field components [21]. The present observation suggests that the excitation bands of Ce^{3+} in α-Sialon are seriously overlapping and/or that some of them maybe located in the conduction band of the host lattice. Under the

excitation of 383 nm, $Ca_{0.84}Ce_{0.08}Li_{0.08}Si_9Al_3ON_{15}$ shows a typical broad emission of Ce^{3+} with maximum at about 502 nm, and the full width at half-maximum (FWHM) is about 112 nm. After Gaussian deconvolution, the broad emission band can be well decomposed into two components centered at about 486 and 536 nm (see the inset in Fig. 5) with an energy difference of about 1920 cm^{-1} corresponding favorably to the splitting of the $4f^1$ ground sate configuration of the Ce^{3+} ion (the energy difference between $^2F_{7/2}$ and $^2F_{5/2}$ levels normally is about 2000 cm^{-1}) [21]. Additionally, varying the excitation wavelength from 287, 383, to 400 nm, the shape and position of the emission spectra almost cannot be changed except for the intensity, which suggests the presence of only one kind of emission center of the Ce^{3+} ions in α-Sialon host lattice. Similar photoluminescent spectra have also been observed by Krevel and Xie et al. [1,24,25] in (Ca,Ce)-α-Sialon.

3.4. Effect of cerium concentration on photoluminescence properties

Fig. 6(a) gives the variation of normalized excitation and emission spectra of phosphors consisting of $m=2.0$ and $n=1.0$ with x values. A redshift of about 14–18 nm in the excitation and emission spectra can be observed when the x value (Ce^{3+} concentration) increases from 0.02 to 0.25. The maximum of the main excitation band prolongs from 378 to 392 nm, and the corresponding emission band shifts from 500 to 518 nm. This shift may come from two reasons: one is some changes in the crystal field around Ce^{3+} which causes the splitting of 5d electrons. As we know, the probability of the energy transfer from the Ce^{3+} ions at higher levels of 5d to those at lower levels of 5d increases with an increase of cerium concentration. This makes it possible that higher Ce concentration lowers the emission energy for transfer from the low 5d excited state to the 4f ground state, and hence the emission shifts to long wavelength; the other is the contribution of reabsorption caused by overlapping absorption and emission bands. The similar dependence of excitation and emission intensities on the cerium concentrations is present in Fig. 6(b). The highest PL intensity is found at $x=0.08$–0.10, above which concentration quenching occurs. The concentration quenching frequently appears in rare-earth-doped phosphors as the dopant increases [4,14,19,26–28]. It is often ascribed to the increase in nonradiative energy transfer among Ce^{3+} ions as the x value increases, which may be caused by electric multipolar interaction and radiation reabsorption.

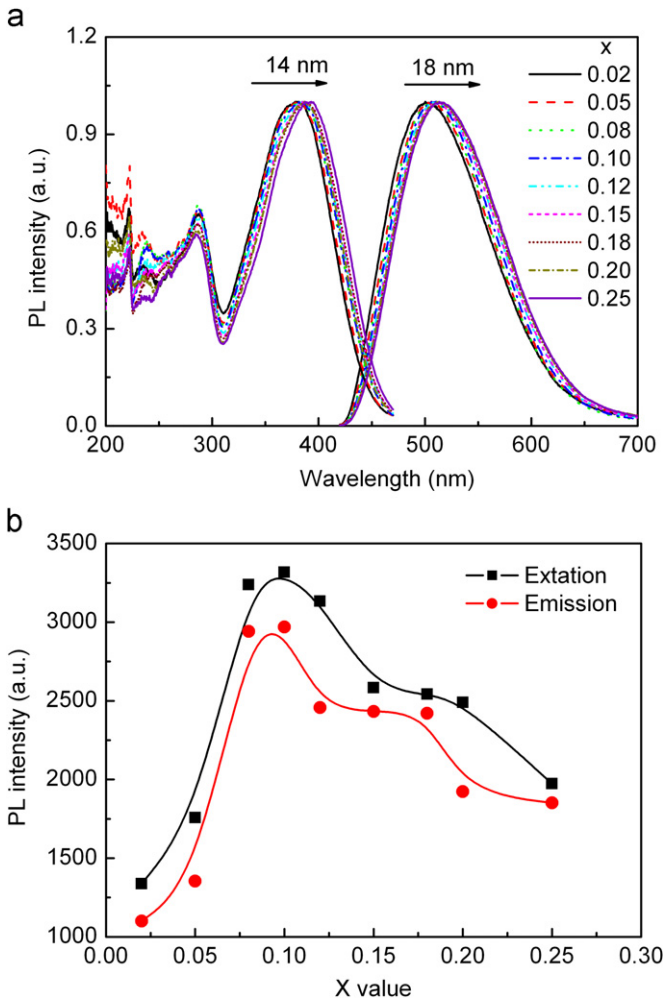

Fig. 6. The normalized excitation and emission spectra (a) and photoluminescence intensities (b) of phosphors ($m=2.0$ and $n=1.0$) with varing x values (Ce^{3+} concentrations).

3.5. Effect of host lattice composition on photoluminescence properties

As we know, the crystal structure of α-Sialon can remain unchanged when the chemical compositions of host lattice alter in a wide range by adjusting m and n values. This allows for more freedom of the compositional design, which finally causes the variation of optical properties. Based on this case, the photoluminescent intensity and the peak wavelength as a function of the composition of the α-Sialon host matrix are shown in Fig. 7. The strongest luminescence is achieved at about $m=2.0$–2.5 when the n value and the relative concentration of Ce^{3+} are fixed at 1.0 and 8 at%, respectively (Fig. 7(a)). The variation of intensity with m value is mainly dependent on the phase purity and the absolute concentration of Ce^{3+}. The impurity phase AlN begins to form when m value is above 2.5 (see Fig. 2(a)), which may be one reason to lead the decrease of the intensity. On the other hand, from the theoretical composition formula of α-Sialon, we can see that the absolute concentration of Ce^{3+} ($x\times m/2$) increases with the increase of m, and thus concentration quenching occurs at $m>2.5$. Additionally, the emission band shows a slight redshift of 7 nm with the m value increasing from 0.5 to 3.5, see the inset in Fig. 7(a). This shift is similar to the influence of Ce^{3+} concentration on the position of the emission band and is also attributed to changes in the crystal field around Ce^{3+} and the reabsorption between Ce^{3+} because of the increase of the absolute concentration. Simultaneously, the corresponding excitation band exhibits an obvious redshift of 24 nm. The reason is still unclear; the shift of the excitation band at a wide range, however, implies that the luminescent properties of Ca-α-Sialon:Ce^{3+},Li^+ can be tailored by controlling the overall composition of the host lattice to perfectly match with the near-UV LEDs in the range of 360–410 nm.

When the m value is fixed at 2.0, the luminescent intensity enhances as n value increases up to 1.0–1.2, and then it falls with higher n value (Fig. 7(b)). The photoluminescence intensities of Ca-α-Sialon:Ce^{3+},Li^+ with various n values are mainly dependent on phase purity, crystallinity, and particle morphology. With the lower n values (i.e. 0.16), phosphor particles basically have bad crystallinity and a smaller size of about several hundred nanometers due to a smaller amount of transient liquid phase during the firing, as shown in Fig. 8(a). Defects in each particle could trap or scatter the emitting light, which finally reduces the luminescence. For higher n value, crystal grains gradually grow, and a relative uniform and dispersive morphology are present at $n=1.0$ (Fig. 3). Thus, the strongest luminescence is observed. With n value increasing continuously to 2.0, the crystal easily grains agglomerate (Fig. 8(b)) and the impurity phase of $SiAl_8O_2N_8$ simultaneously forms and coexists with α-Sialon, which would consequently reduce the packing density and phase purity of the

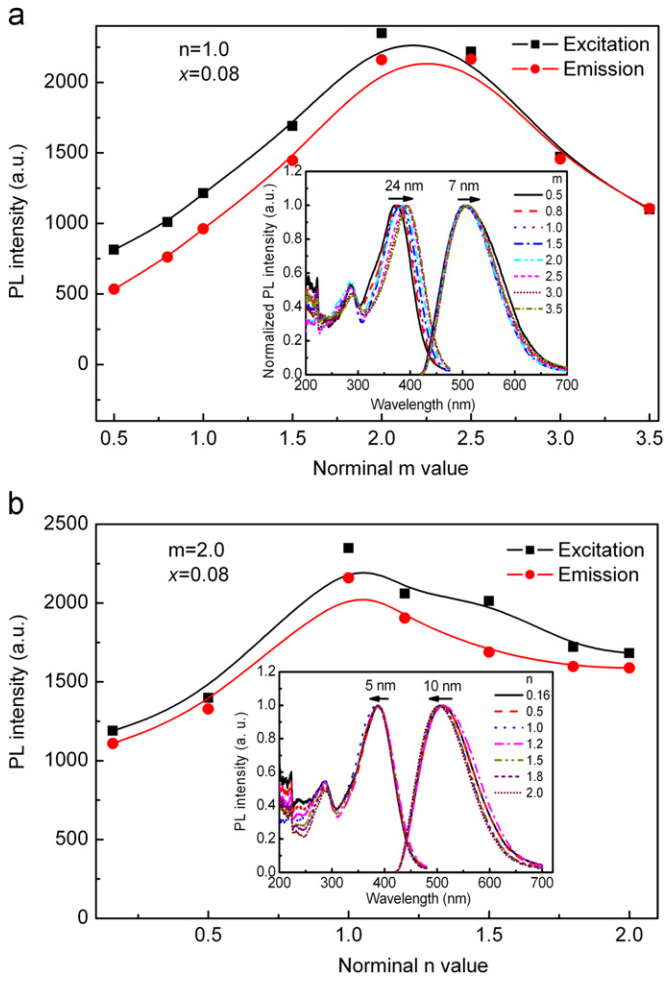

Fig. 7. Dependence of photoluminescence intensity and normalized photoluminescence spectra (the inset) on the host lattice composition: (a) m value and (b) n value.

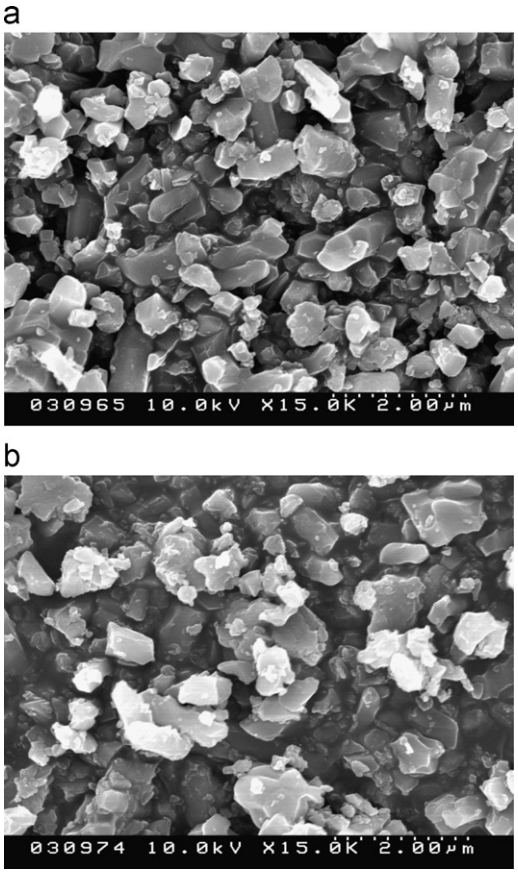

Fig. 8. SEM micrographs of phosphors with different n values: (a) 0.16 and (b) 2.0.

powder, and finally causes a strong scattering of the light. Another interesting feature relating to the increase of n value is a small blueshift (5–10 nm) of the excitation and emission bands (see the inset in Fig. 7(b)). This blueshift is caused by the reduction on the covalence of chemical bonds due to the increase of O/N ratio when n value is enhanced.

3.6. Quantum efficiency

Fig. 9 reveals the external QE and absorption (inset) of Ca-α-Sialon:Ce^{3+},Li^{+} phosphor with different m and n values as a function of the excitation wavelength. As seen, the absorption increases with m value increasing from 0.5 to 3.0 due to the increase of the absolute concentration of Ce^{3+} ($x \times m/2$); however, it almost keeps unchanged as n value varies. The external QE reaches the highest value at $m=2.0$ and $n=1.0$ in the whole excitation wavelength of 300–450 nm, which is consistent with the variation of photoluminescence intensity. In this case, the external QE is about 35% at $\lambda_{ex}=380$ nm.

3.7. Temperature-dependent luminescence and chromaticity

Temperature-dependent luminescence of Ca-α-Sialon:Ce^{3+},Li^{+} with various m and n values ($x=0.08$) was investigated at temperatures ranging from 25 to 300 °C, as seen in Fig. 10. Clearly the emission intensity of all samples falls as the temperature rises. The thermal quenching is strongly related to the m and n values. It enhances with the increase in the m value when x and n is fixed at 0.08 and 1.0, respectively. This phenomenon could be explained by the increment of the probability of nonradiative transition and the reabsorption among Ce^{3+} ions caused by its absolute concentration increasing ($x \times m/2$), which can also be observed in the absorption spectra (the inset of Fig. 9(a)). Additionally, the increase in the m value reduces the stiffness of the crystal structure because of the smaller bond energy of Al–N (2.88 eV) in AlN as compared to that of Si–N (4.52 eV) in Si_3N_4 [29,30], which also contributes to the large thermal quenching of phosphors with the large m value. Fixing $m=2.0$ and $x=0.08$, the thermal quenching decreases with the increment of n value from 0.16 to 1.0, which is in good agreement with the variation of luminescent intensity with n value (Fig. 7(b)). The thermal quenching of phosphors is usually affected by many factors, such as the rigidity of the crystal structure, crystallinity, defect levels, Stokes shift, etc. Fig. 2(b) shows that the lattice volume of α-Sialon remains almost unchanged with increasing n. Thus the influence of the rigidity of the crystal structure on the thermal quenching of phosphors with different n value is negligible. In this case, the mechanism for the thermal quenching of Ca-α-Sialon:Ce^{3+},Li^{+} ($m=2.0$ and $x=0.08$) may be mainly due to the crystallinity, defect levels, and Stokes shift. The increase in the n value (i.e., the enhanced O/N ratio) improves crystallinity or particle size, optimizes morphology (see Figs. 3 and 8), decreases the defect levels, and finally results in the higher thermal stability. Meanwhile, the increase of n value leads to a slight blueshift of the emission band (see the inset in Fig. 7(b)), indicating that the Stokes shift decreases as n increases, which may also contribute to the high thermal stability of phosphors with large n value. At 150 °C, emission intensities of all samples maintain above 85% of that

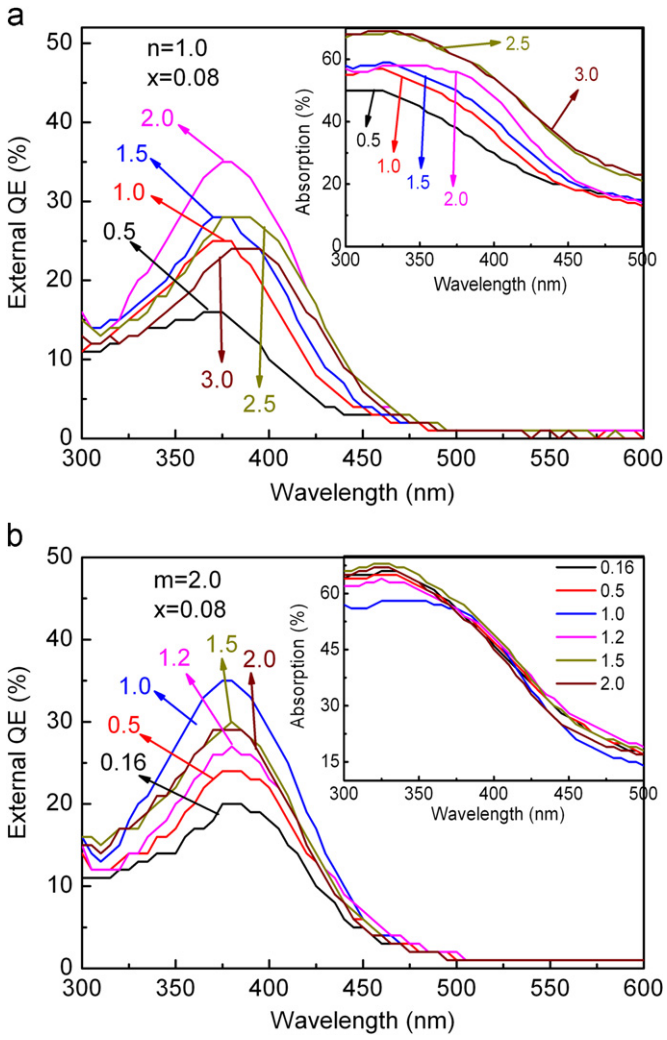

Fig. 9. The external QE and absorption (inset) of Ca-α-Sialon:Ce^{3+},Li^{+} with different m (a) and n (b) values.

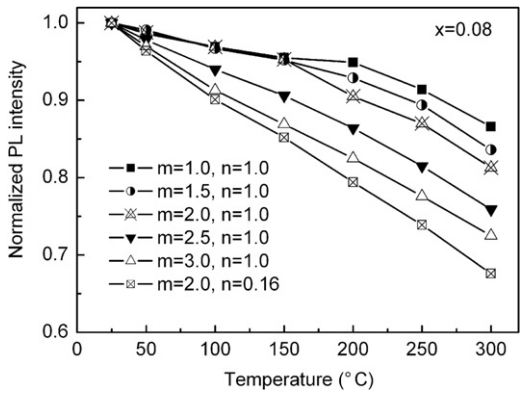

Fig. 10. Temperature-dependent luminescence of Ca-α-Sialon:Ce^{3+},Li^{+} with varying m and n values.

measured at room temperature, indicative of a high thermal stability of Ca-α-Sialon:Ce^{3+},Li^{+} phosphors. The small thermal quenching is an important requirement for phosphors to reduce the variations in chromaticity and brightness of white LEDs at high temperature [31].

The temperature-dependent emission spectra of Ca-α-Sialon:Ce^{3+},Li^{+} phosphor with the composition of $x=0.08$, $m=2.0$, and $n=1.0$ are shown in Fig. 11. No obvious shift is observed in the

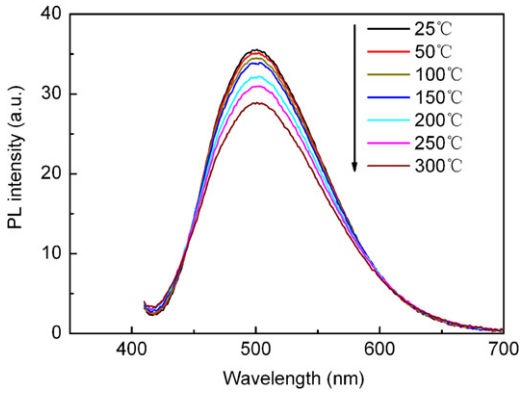

Fig. 11. Temperature-dependent emission spectra of Ca-α-Sialon:Ce^{3+},Li^{+} with $m=2.0$, $n=1.0$, and $x=0.08$.

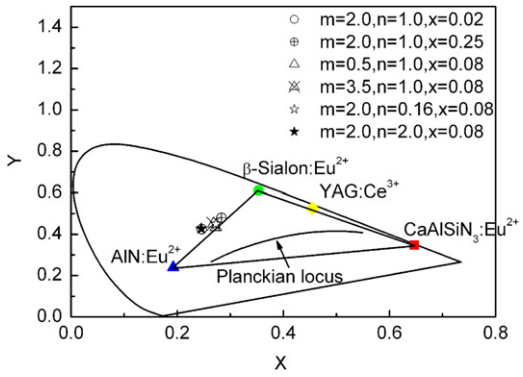

Fig. 12. Chromatic coordinates of Ca-α-Sialon:Ce^{3+},Li^{+} phosphors with different compositions. The chromaticity of YAG:Ce^{3+} (P46-Y3, yellow) and typical RGB phosphors ($CaAlSiN_3$:Eu^{2+}—Red, β-Sialon:Eu^{2+}—Green and AlN:Eu^{2+}—Blue) is also included. The blackbody radiation locus is indicated by the solid curve. (For interpretation of the references to color in this figure legend, the reader is referred to the web version of this article.)

emission band except for the decrease of intensity when the temperature rises, suggesting the stable chromaticity coordinates of this host phosphors by varying the temperature. The CIE (Commission International del'Eclairge) 1931 chromaticity of Ca-α-Sialon:Ce^{3+},Li^{+} with different compositions is present in Fig. 12. We can see that the chromatic points of Ca-α-Sialon:Ce^{3+},Li^{+} with different compositions all locate at the region between blue and green parts, and it shifts to green with increasing Ce^{3+} concentration and m value. However, when m and x values are fixed, the chromatic point shifts to the blue with the increase of n value. This variation is consistent with the PL spectra in Figs. 6 and 7, and also indicates that the chromaticity of Ca-α-Sialon:Ce^{3+},Li^{+} can be adjusted by controlling the overall composition of the host lattice to make white LED devices with different correlated color temperature (CCT) and color rendering index (CRI) by combining with additional yellow (YAG:Ce^{3+}) or red ($CaAlSiN_3$:Eu^{2+}) phosphors.

4. Conclusions

We have successfully synthesized a green-blue emission phosphor Ca-α-Sialon:Ce^{3+},Li^{+} with compositions of $[Ca_{(1-2x)}\ Ce_xLi_x]_{m/2}Si_{12-(m+n)}Al_{m+n}O_nN_{16-n}$ ($0\le x\le 0.25$, $0.5\le m\le 3.5$, and $0.16\le n\le 2.0$) by a solid-state reaction at 1700 °C under a nitrogen gas pressure of 0.5 MPa. The effects of the activator concentration and the overall composition of host lattice on the phase evolution and optical properties such as excitation and emission spectra, QE, and thermal

quenching have been discussed. A single-phase Ca-α-Sialon:Ce^{3+},Li^{+} phosphor can be synthesized at $x<0.1$, $1.0\leq m\leq 2.5$, and $n\leq 1.2$. The photoluminescence properties can be tailored by controlling Ce^{3+} concentration and the overall composition of the α-Sialon host lattice. With increasing the Ce concentration and m value both excitation and emission bands show a red shift, which perfectly matches with the near-UV LEDs in the range of 360–410 nm. The strongest luminescence is achieved at $x=0.08$–0.1, $m=2.0$–2.5, and $n=1.0$. Simultaneously, the highest QE and better thermal stability are also present.

Acknowledgments

The authors gratefully acknowledge financial supports from National Natural Science Foundation of China (No. 50902050), the Fundamental Research Funds for the Central Universities (No. 78210002), Shanghai Baiyulan Foundation (No. 2010B026), and Special Project for Solid-State Lighting Engineering and Optoelectronics of Shanghai (No. 09DZ1141900).

References

[1] J.W.H. van Krevel, J.W.T. Rutten, H. Mandal, H.T. Hintzen, R. Metselaar, J. Solid State Chem. 165 (2002) 19.
[2] R.-J. Xie, M. Mitomo, K. Uheda, F.-F. Xu, Y. Akimune, J. Am. Ceram. Soc. 85 (5) (2002) 1229.
[3] R.-J. Xie, N. Hirosaki, M. Mitomo, Y. Yamamoto, T. Suehiro, J. Phys. Chem. B 108 (2004) 12027.
[4] R.-J. Xie, N. Hirosaki, K. Sakuma, Y. Yamamoto, M. Mitomo, Appl. Phys. Lett. 84 (2004) 5404.
[5] K. Sakuma, K. Omichi, N. Kimura, M. Ohashi, D. Tanaka, N. Hirosaki, Y. Yamamoto, R.-J. Xie, T. Suehiro, Opt. Lett. 29 (2004) 2001.
[6] R.-J. Xie, N. Hirosaki, M. Mitomo, K. Takahashi, K. Sakuma, Appl. Phys. Lett. 88 (2006) 101104.
[7] R.-J. Xie, N. Hirosaki, M. Mitomo, K. Sakuma, N. Kimura, Appl. Phys. Lett. 89 (2006) 241103.
[8] K. Sakuma, N. Hirosaki, R.-J. Xie, J. Lumin. 126 (2007) 843.
[9] K. Sakuma, N. Hirosaki, R.-J. Xie, Y. Yamamoto, T. Suehiro, Mater. Lett. 61 (2007) 547.
[10] N. Kimura, K. Sakuma, S. Hirafune, K. Asano, N. Hirosaki, R.-J. Xie, Appl. Phys. Lett. 90 (2007) 051109.
[11] H.-L. Li, R.-J. Xie, N. Hirosaki, T. Suehiro, Y. Yajima, J. Electrochem. Soc. 155 (2008) J175.
[12] L. Liu, R.-J. Xie, N. Hirosaki, T. Takeda, J. Li, X. Sun, J. Am. Ceram. Soc. 92 (11) (2009) 2668.
[13] K. Sakuma, N. Hirosaki, N. Kimura, Y. Yamamoto, R.-J. Xie, T. Suehiro, K. Omichi, M. Ohashi, D. Tanaka, in: Proceedings of the IDW'04 PHp-1, 2004, pp. 1115.
[14] R.-J. Xie, N. Hirosaki, M. Mitomo, K. Uheda, T. Suehiro, X. Xu, Y. Yamamoto, T. Sekiguchi, J. Phys. Chem. B 109 (2005) 9490.
[15] J.W.H. van Krevel, H.T. Hintzen, R. Metselaar, A. Meijerink, J. Alloy Compd. 268 (1998) 272.
[16] Y.Q. Li, G. de With, H.T. Hintzen, J. Mater. Chem. 15 (2005) 4492.
[17] R. Le Toquin, A.K. Cheetham, Chem. Phys. Lett. 423 (2006) 352.
[18] Y.Q. Li, G. de With, H.T. Hintzen, J. Lumin. 116 (2006) 107.
[19] L. Liu, R.-J. Xie, N. Hirosaki, T. Takeda, C.-N. Zhang, J. Li, X. Sun, J. Electrochem. Soc. 157 (1) (2010) H50.
[20] Y.Q. Li, N. Hirosaki, R.J. Xie, J. Li, T. Takeda, Y. Yamamoto, M. Mitomo, J. Am. Ceram. Soc. 92 (11) (2009) 2738.
[21] G. Blasse, B.C. Grabmaier, Luminescent Materials, Springer, Berlin, 1994.
[22] J.W.H. van Krevel, H.T. Hintzen, R. Metselaar, Mater. Res. Bull. 35 (2000) 747.
[23] B. Dierre, R.-J. Xie, N. Hirosaki, T. Sekiguchi, J. Mater. Res. 22 (2007) 1933.
[24] R.-J. Xie, N. Hirosaki, M. Mitomo, Y. Yamamoto, T. Suehiro, N. Ohashi, J. Am. Ceram. Soc. 87 (7) (2004) 1368.
[25] R.-J. Xie, N. Hirosaki, M. Mitomo, T. Suehiro, X. Xu, H. Tanaka, J. Am. Ceram. Soc. 88 (10) (2005) 2883.
[26] H.-L. Li, R.-J. Xie, N. Hirosaki, Y. Yajima, J. Electrochem. Soc. 155 (2008) J378.
[27] H.-L. Li, R.-J. Xie, N. Hirosaki, B. Dierre, T. Sekiguchi, Y. Yajima, J. Am. Ceram. Soc. 91 (2008) 1711.
[28] H.-L. Li, R.-J. Xie, G.-H. Zhou, N. Hirosaki, Z. Sun, J. Electrochem. Soc. 157 (2010) J251.
[29] H. Maruo, I. Miyamoto, T. Ooie, J. Jpn. Welding Soc. 10 (1992) 439.
[30] T. Wang, K.B. Lee, J. Bai, P.J. Parbrook, F. Ranalli, Q. Wang, R.J. Airey, D.G. Cullis, H.X. Zhang, D. Massoubre, Z. Gong, I.M. Watson, E. Gu, M.D. Dawson, J. Phys. D: Appl. Phys. 41 (2008) 094003.
[31] Y.-S. Tang, S.-F. Hu, C.C. Lin, N.C. Bagkar, R.-S. Liu, Appl. Phys. Lett. 90 (2007) 151108.